Interfacial Electronic Structure in Thiolate Self-Assembled Monolayers: Implication for Molecular Electronics

T. Vondrak, H. Wang, P. Winget, C. J. Cramer, and X.-Y. Zhu*

Contribution from the Department of Chemistry & Supercomputer Institute, University of Minnesota, Minneapolis, Minnesota 55455

Received September 27, 1999

Abstract: Thiolate self-assembled monolayers (SAMs) on metal surfaces have been explored recently to address the assembly and connection issue in molecular electronics. In these systems, the molecule−metal contact is detrimental to electron transport. This is manifested not only in contact resistance, but also in the nature of the molecular device, which depends on the extent of wave function mixing between the molecule and the metal surface. We probe interfacial electronic structure, particularly unoccupied electronic states, in thiolate SAMs on Cu(111) using laser two-photon photoemission spectroscopy, in conjunction with ab initio calculations of model molecules. We find that the interfacial electronic structure is dominated by two virtual orbitals localized to the thiolate anchor and strongly coupled to the metal substrate. The shapes and energies of these interfacial σ^*-like orbitals are independent of the nature of the hydrocarbon group (conjugated aromatics or saturated alkyls). As low-lying acceptor orbitals, they may play important roles in electron transport through self-assembled molecular wires.

1. Introduction

With the continuing trend of miniaturization in conventional electronic devices, physical limits will soon be reached. An exciting alternative is single-electron devices, which are based on the Coulomb blockade of electron transport when charge is confined to a nanometer scale island.[1−3] While many single-electron devices have been demonstrated at cryogenic temperatures, application at room temperature would require that the size of these metal or semiconductor islands (*quantum dots*) be smaller than 10 nm. Fabricating solid structures with <10 nm features on a large scale is a formidable technological challenge. On the other hand, this is within the scale of a simple molecule. Indeed, molecular single electron devices, including room temperature transistors, have been demonstrated recently using carbon nanotubes attached to nanoscale metal electrodes.[4−6] An attractive alternative to carbon nanotubes is the use of other organic molecules, such as conjugated oligomers and aromatic molecules, as single-electron transport devices. This is because the easy incorporation of functional groups and the availability of a large repertoire of synthetic techniques facilitates the rational design and assembly of molecular electronic devices.

There are at least two chemical issues in building a molecular electronic device: (i) the design and synthesis of useful organic molecules and (ii) the assembly of these molecules into devices and their connection to the macroscopic world. The first issue is most promising, thanks to the power of modern synthetic techniques[7] and ever more accurate theoretical models. The assembly and connection issue is more difficult. Traditional techniques from organic synthesis are not necessarily applicable when a large number of molecules are concerned. A preferred approach would rely on molecular self-assembly, such as self-assembled monolayers (SAMs).[8,9] An obvious benefit of covalent attachment to metal and semiconductor surfaces in SAMs is that connection to the outside world can be easily achieved. A number of groups have studied electron transport in single molecules using thiolate SAMs on gold surfaces.[10−14] For example, Reed et al. measured electron transport in benzene-1,4-dithiol ($HS-C_6H_4-SH$) self-assembled onto two adjacent Au electrodes of a mechanically controllable break junction and suggested the possibility of a Coulomb blockade.[12] Using scanning tunneling microscopy (STM), Dhirani et al. found a rectifying effect in a SAM of conjugated $C_6H_5-C\equiv C-C_6H_4-C\equiv C-C_6H_4-SH$ on Au,[13] while Weiss and co-workers reported enhanced conductivity of similar molecules inserted into SAMs of alkanethiolate on Au(111).[10,11] Datta and co-workers measured the current−voltage characteristics in STM for α,α'-xylyl dithiol ($HS-CH_2-C_6H_4-CH_2-SH$) self-assembled on Au and compared experiment with simulation based on the scattering theory of transport.[14]

* Address correspondence to this author. Phone: (612) 624-7849. Fax: (612) 626-7541. E-mail: zhu@chem.umn.edu.

(1) Dvoret, M. H.; Esteve, D.; Urbina, C. *Nature* **1992**, *360*, 547.
(2) Kastner, M. *Phys. Today* **1993**, *46*, 24.
(3) Ashoori, R. C. *Nature* **1996**, *379*, 413.
(4) Chico, L.; Crespi, V. H.; Benedict, L. X.; Louie, S. G.; Cohen, M. L. *Phys. Rev. Lett.* **1996**, *76*, 971.
(5) Tans, S. J.; Devoret, M. H.; Dai, H.; Thess, A.; Smalley, R. E.; Geerlings, L. J.; Dekker, C. *Nature* **1997**, *386*, 474.
(6) Tans, S. J.; Verschueren, A. R. M.; Dekker, C. *Nature* **1998**, *393*, 49.
(7) Tour, J. M. *Chem. Rev.* **1996**, *96*, 537.
(8) Dubois, L. H.; Nuzzo, R. G. *Annu. Rev. Phys. Chem.* **1992**, *43*, 437.
(9) Ulman, A. *Chem. Rev.* **1996**, *96*, 1533.
(10) Bumm, L. A.; Arnold, J. J.; Cygan, M. T.; Dunbar, T. D.; Burgin, T. P.; Jones, L., II; Allara, D. L.; Tour, J. M.; Weiss, P. S. *Science* **1996**, *271*, 1705.
(11) Cygan, M. T.; Dunbar, T. D.; Arnold, J. J.; Bumm, L. A.; Shedlock, N. F., Burgin, T. P.; Jones, L., II; Allara, D. L.; Tour, J. M.; Weiss, P. S. *J. Am. Chem. Soc.* **1998**, *120*, 2721.
(12) Reed, M. A.; Zhou, C.; Muller, C. J.; Burgin, T. P.; Tour, J. M. *Science* **1997**, *278*, 252.
(13) Dhirani, A.-A.; Lin, P. H.; Guyot-Sionnest, P.; Zehner, R. W.; Sita, L. R. *J. Chem. Phys.* **1997**, *106*, 5249.
(14) Datta, S.; Tian, W.; Hong, S.; Reifenberger, R.; Henderson, J. I.; Kubiak, C. P. *Phys. Rev. Lett.* **1997**, *79*, 2530.

10.1021/ja993486w CCC: $19.00
Published on Web 04/29/2000

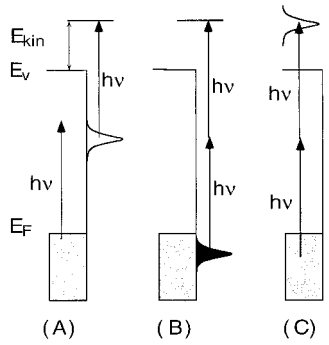

Figure 1. Three scenarios in two-photon photoemission: (A) 2PPE involving an unoccupied resonance, in which electron energy scales with one photon energy, i.e., $\Delta E_{kin} = \Delta h\nu$; (B) two photon excitation from an occupied state, $\Delta E_{kin} = 2\Delta h\nu$; and (C) two photon excitation into a final state, E_{kin} independent of $h\nu$. E_F = Fermi level; E_V = vacuum level.

In all self-assembled molecular electronics, the contact between the molecule and the metal electrode is detrimental to electron transport through a single molecule. This is manifested not only in contact resistance, but also in the nature of the molecular device, which depends on the extent of wave function mixing between the molecule and the substrate. On the molecular level, charge transport across the interface is governed by the electronic interaction between the molecule and the surface.[15] This interaction determines both energetics and dynamics. Thus, understanding and controlling the electronic interaction between a molecule and the substrate is critical in designing all electronic and optoelectronic devices based on organic molecules. There have been a number of theoretical studies on the interfacial electronic structure in thiolate SAMs,[16−19] but experimental data are largely unavailable.

Here, we report systematic efforts to establish interfacial electronic structures, particularly unoccupied states, in thiolate SAMs using laser two-photon photoemission (2PPE) spectroscopy.[20] Unlike conventional ultraviolet photoemission spectroscopy (UPS), which probes occupied electronic states, laser 2PPE probes both occupied and unoccupied states. Unoccupied electronic states are of equal importance as occupied states, e.g., in electron injection from metal electrodes into conduction bands of organic layers or in resonant electron transport via the lowest unoccupied molecular orbital (LUMO) in single-molecule devices. A particularly exciting aspect of 2PPE is that it can be carried out in a time-resolved manner using femtosecond laser pulses[21−24] to directly measure the ultrafast electron transfer rate between molecular states and the metal surface. Figure 1 shows schematically three possible scenarios in 2PPE. In Fiugre 1A, the absorption of photons creates hot substrate electrons which can tunnel to an unoccupied state localized at the surface; the absorption of a second photon excites this transient electron above the vacuum level. In this case, the change in electron kinetic energy scales with that in photon energy, i.e., $\Delta E_{kin} = 1\cdot\Delta h\nu$. 2PPE can also probe occupied states, Figure 1B, in which coherent two-photon excitation from a state below the Fermi level leads to the ejection of one electron. This is similar to conventional UPS, except that $\Delta E_{kin} = 2\cdot\Delta h\nu$. Finally, if the unoccupied state is above the vacuum level, Figure 1C, E_{kin} is independent of photon energy. 2PPE has been used successfully in characterizing the energetics and dynamics of image states on metal surfaces.[21−24] The use of 2PPE in characterizing adsorbate resonances and dynamics has also been reported.[25−31]

We choose Cu(111) because it is the best characterized surface in recent 2PPE studies[20−31] and these may serve as valuable points of reference. Thiolate SAMs are known to form on all coinage metals, including Cu(111), although the majority of studies have used Au(111) due to the stability of this surface under ambient conditions.[9] We investigate three thiolate self-assembled monolayer systems: thiophenolate, octylthiolate, and ethylthiolate. The thiophenolate (C_6H_5S-) system represents the simplest model interface for SAMs of molecular "wires". This system is compared to two alkylthiolates with different alkyl chain lengths, octylthiolate (n-$C_8H_{17}S-$) and ethylthiolate (n-C_2H_5S-). We found that the interfacial electronic structure is independent of the nature of the hydrocarbon group; all surfaces are characterized by two virtual states localized to the C−S−Cu anchor.

2. Experimental Section

All experiments were performed in an ultrahigh vacuum (UHV) chamber pumped by a turbo molecular pump, with a base pressure of 1×10^{-10} Torr. The system consisted of two levels. The upper level was equipped with a low-energy electron diffraction (LEED) and Auger electron spectrometer (AES) for surface analysis, an ion sputtering gun for surface cleaning, and a quadrupole mass spectrometer (QMS) for gas analysis.

Two-photon photoemission (2PPE) spectra were recorded at the lower level of the UHV chamber on a homemade time-of-flight (TOF) spectrometer, which was made of all copper material. The entrance to the flight tube was a nozzle with a ϕ 1.5 mm opening. The total flight distance (field-free region) was d = 30 cm. Electrons were detected by Chevron multichannel plates with a ϕ 40 mm active area. The signal from the anode was coupled out via a vacuum compatible capacitor (270 pF) mounted on the back of the anode and, after preamplification, recorded by a multichannel scaler (MCS) with 5 ns resolution (EG&G). The TOF spectrometer was shielded by a magnetic shield. The Cu sample was inserted through a hole on the top of the magnetic shield and positioned 1−2 mm from the opening of the flight tube. Laser light for 2PPE was from a tunable dye laser (Continuum ND6000) pumped by a Q-switched Nd:YAG laser (Continuum Powerlite 7010). The UV output was passed through an iris (ϕ 1 mm) and a quartz window and directed at the sample surface at 60° from surface normal. Polarization of the incident light was controlled by a half-wave plate. For p-polarization, the electric field vector was in the plane-of-incidence (defined by the directions of light propagation and surface normal). For s-perpendicular, it was perpendicular to the plane-of-incidence. In most measurements, the sample was normal to the center axis of the flight tube, i.e., zero parallel momentum, and the reflected light exited

(15) Miller, R. J. D.; McLendon, G. L.; Nozik, A. J.; Schmickler, W.; Willig, F. *Surface electron-transfer processes*; VCH: New York, 1995.
(16) Magoga, M.; Joachim, C. *Phys. Rev. B* **1997**, *56*, 4722.
(17) Yaliraki, S. Y.; Ratner, M. A. *J. Chem. Phys.* **1998**, *109*, 5036.
(18) Yaliraki, S. Y.; Kemp, M.; Ratner, M. A. *J. Am. Chem. Soc.* **1999**, *121*, 3428.
(19) Seminario, J. M.; Zacarias, A. G.; Tour, J. M. *J. Am. Chem. Soc.* **1999**, *121*, 411.
(20) Fauster, Th.; Steinmann, W. In *Photonic probes of surfaces*; Halevi, P., Ed.; Elsevier: Amsterdam, 1995.
(21) Harris, C. B.; Ge, N. H.; Lingle, R. L.; McNeill, J. D.; Wong, C. M. *Annu. Rev. Phys. Chem.* **1997**, *48*, 711.
(22) Petek, H.; Ogawa, S. *Prog. Surf. Sci.* **1998**, *56*, 239.
(23) Wolf, M.; Knoesel, E.; Hertel, T. *Phys. Rev. B* **1996**, *54*, R5296.
(24) Hofer, U.; Shumay, I. L.; Reuss, Ch.; Thomann, U.; Wallauer, W.; Fauster, Th. *Science* **1997**, *277*, 1480.
(25) Hertel, T.; Knoesel, E.; Hasselbrink, E.; Wolf, M.; Ertl, G. *Surf. Sci.* **1994**, *317*, L1147.
(26) Knoesel, E.; Hertel, T.; Wolf, M.; Ertl, G. *Chem. Phys. Lett.* **1995**, *240*, 409.
(27) Bauer, M.; Pawlik, S.; Aeschlimann, M. *Phys. Rev. B* **1997**, *55*, 10040.
(28) Ogawa, S.; Nagano, H.; Petek, H. *Phys. Rev. Lett.* **1999**, *82*, 1931.
(29) Velic, D.; Hotzel, A.; Wolf, M.; Ertl, G. *J. Chem. Phys.* **1998**, *105*, 9155.
(30) Vondrak, T.; Zhu, X.-Y. *J. Phys. Chem.* **1999**, *103*, 3449.
(31) Vondrak, T.; Cramer, C. J.; Zhu, X.-Y. *J. Phys. Chem.* **1999**, *103*, 8915.

the UHV chamber through a UV window. In dispersion measurements, the angle between surface normal and the center axis of the flight tube was varied between 0 and 20°. Note that the MCS was triggered by the synchronized output from the Q-switch. Zero time was determined precisely by the arrival time of signal from a small amount of intentionally scattered laser light. In most measurements, a typical laser pulse energy density of 1−3 mJ/cm^2 was used. There was no space charge problem in this power density region. All 2PPE measurements were carried out at a surface temperature of 298 K.

The Cu(111) sample (ϕ 10 mm, polished to within 1° of the ⟨111⟩ direction) was mounted at the center of the chamber on a sample manipulator. It was cooled by liquid nitrogen and heated resistively through two tungsten wires mounted on the edge of the sample. Temperature was measured by a type K thermocouple inserted into a small hole on the edge of the Cu crystal. Cleaning was achieved by repeated cycles of Ar^+ sputtering (1.5 keV) and annealing (775 K) to yield a sharp (1 × 1) LEED pattern. The clean surface was further confirmed by AES.

Three thiol molecules (Aldrich 99+%) were used in this study, including thiophenol (C_6H_5SH), octylthiol (n-$C_8H_{17}SH$), and ethylthiol (n-C_2H_5SH), which were purified by freeze−pump−thaw cycles. The self-assembled monolayers were formed by dosing corresponding thiol molecules onto the Cu(111) surface at a substrate temperature of 300 K, with total exposure exceeding 10^4 Langmuir (L). Recent studies of alkylthiol SAMs on Au(111) showed the formation of a saturated 2D crystalline phase at gas exposures $\geq 2 \times 10^3$ L.[32] Although the majority of studies have concentrated on Au, thiol SAMs also form on Cu-(111).[9,33] Thiophenolate is known to form SAM on metal surfaces.[34−38] Despite the lack of long range order, each C_6H_5−S− is believed to be oriented with a tilt angle of ∼25° from surface normal.[37]

3. Results and Discussions

We organize results and discussions into four sections. In section 3.1, we present 2PPE spectra for a SAM of thiophenolate on Cu(111) and show, based on photon energy dependence, the presence of two unoccupied electronic states at the interface. We demonstrate that the same interfacial electronic structure is observed in alkylthiolate SAMs. Section 3.2 summarizes the energetics of the three SAMs systems and concludes that the two unoccupied states must be localized to the Cu−S−C linker. We probe the symmetry of the two transitions using polarized light. In section 3.3, we present ab initio results on model molecules and assign the two unoccupied electronic states to be virtual states localized to the Cu−S−C anchor in SAMs; Finally, in section 3.4, we discuss the implication of these results for molecular electronics.

3.1. Thiophenolate and Alkylthiolate SAMs: Two Unoccupied Electronic States. A self-assembled monolayer of thiophenolate (C_6H_5S−) on metal is a simple model interface for SAMs of conjugated molecular "wires". We establish the interfacial electronic structure using 2PPE. Figure 2 compares a 2PPE spectrum of clean Cu(111) with that from a SAM of C_6H_5S/Cu(111), at a photon energy of 3.70 eV. The spectrum from clean Cu(111) is characterized by three peaks: the peak labeled SS originates from an occupied surface state located at 0.4 eV below the Fermi level, while the two peaks at lower energy are assigned to the Cu d-band (d) and secondary electrons (2nd-e).[22−30] When the Cu(111) surface is covered with C_6H_5S−, the surface state disappears, in agreement with previous studies on chemisorption.[25−28] The spectrum consists of three peaks: the intense d-band/secondary electron peak at low energy (off scale in the figure) and two broad feature above 6.5 eV due to the SAM. The formation of the SAM decreases the surface work function (ϕ) to 3.70 eV, as compared to ϕ = 4.90 eV for clean Cu(111). The decrease in work function is responsible for the substantial increase in secondary electron yield from the SAM covered surface. The SAM related feature can be decomposed into two peaks as shown by the dashed curves (labeled A and B, respectively). In the decomposition, we use Gaussian peak shapes for the two molecular peaks. To facilitate decomposition, we used a mixed Gaussian−Lorentzian function to fit the tail of the secondary/d-band electron peak (dotted line, referred to as background function). Note the positions of both peak A and peak B are insensitive to the details of this background contribution. Similar decomposition procedures (with or without the use of a background function) are used for all spectra taken at different photon energies, as shown below. These decomposition procedures introduce a maximum uncertainty of ±0.1 eV in the position of peak B and ±0.05 eV for peak A. The statistical error from repeated measurements is of the same order.

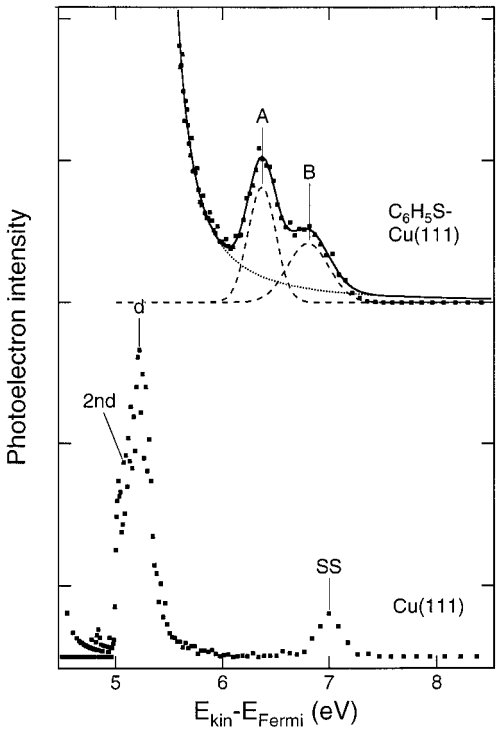

Figure 2. Two-photon photoemission spectra obtained for a self-assembled monolayer (SAM) of C_6H_5S/Cu(111), top, and clean Cu-(111), bottom, at a photon energy of 3.70 eV. Dots are experimental data points. The dashed curves (A and B) on the upper spectrum are from peak decomposition assuming Gaussian peak shapes and the dotted curve is an estimate of the background from secondary electrons (see text for details). The solid curve is the sum of dashed curves and the dotted curve. Note the low-energy region of the spectrum from the SAM covered surface is off-scale, due to very high secondary electron yield. SS = surface state, d = Cu d-band; and 2nd = secondary electrons.

To establish the energetics of these two molecular states, we record the 2PPE spectrum as a function of photon energy. This is shown in Figure 3 for $h\nu$ = 3.44−3.87 eV. The two molecular

(32) Porier, G. E.; Pylant, E. D. *Science* **1996**, *272*, 1145.
(33) Zamborini, F. P.; Campbell, J. K.; Crooks, R. M. *Langmuir* **1998**, *14*, 640.
(34) .Chang, S.-C.; Chao, I.; Tao, Y.-T. *J. Am. Chem. Soc.* **1994**, *116*, 6792.
(35) Tao, Y.-T.; Wu, C.-C.; Eu, J.-Y.; Lin, W.-L.; Wu, K.-C.; Chen, C.-H. *Langmuir* **1997**, *13*, 4018.
(36) Dhirani, A.-A.; Zehner, R. W.; Hsung, R. P.; Guyot-Sionnest, P.; Sita, L. R. *J. Am. Chem. Soc.* **1996**, *118*, 3319.
(37) Jung, H. H., Won, Y. D.; Shin, S.; Kim, K. *Langmuir* **1999**, *15*, 1147.
(38) Stern, D. A.; Wellner, E.; Salaita, G. N.; Laguren-Davidson, L.; Lu, F.; Batina, N.; Frank, D. G.; Zapien, D. C.; Walton, N.; Hubbard, A. T. *J. Am. Chem. Soc.* **1988**, *110*, 4885.

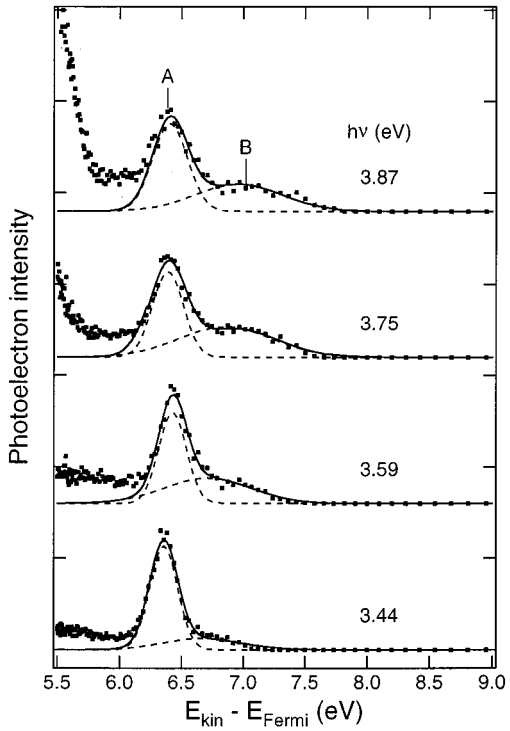

Figure 3. Two-photon photoemission spectra obtained for a self-assembled monolayer (SAM) of C_6H_5S/Cu(111) at the indicated photon energies (3.44−3.87 eV). Dots are experimental data points. The dashed curves (A and B) are from peak decomposition assuming Gaussian peak shapes and the solid curve is the sum of dashed curves. Note that background contribution on the lower energy side of each spectrum is not accounted for in the decomposition (see text for details).

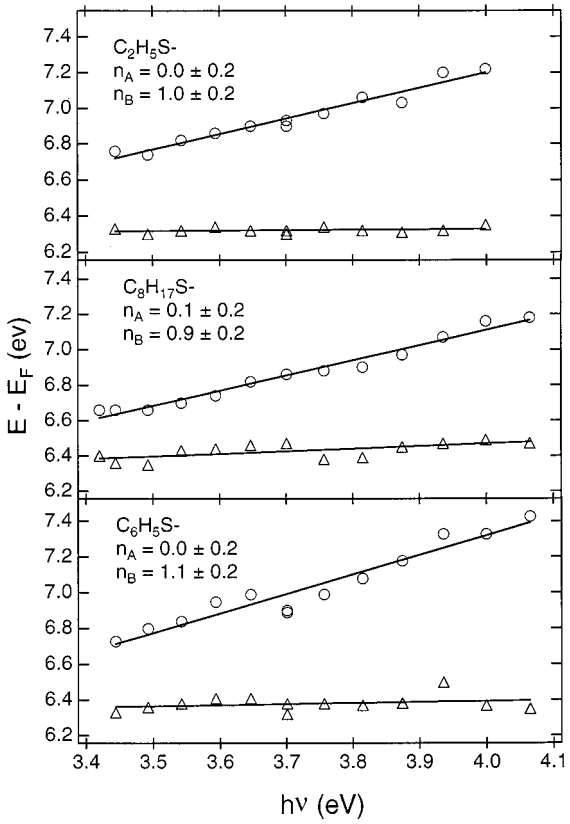

Figure 4. Peak positions for the two spectral features (A, triangles; B, circles) obtained from Gaussian decomposition of two-photon photoemission spectra such as those in Figure 3. The three panels are for SAMs of thiophenolate (bottom), octalthiolates (middle), and ethylthiolate (top), respectively. Two-photon photoemission spectra for octalthiolates and ethylthiolate presented in Figures 5 and 6, respectively. The solid lines are least-squares linear fits which yield the indicated slopes (*n*).

resonances have different photon energy dependences: the position of the first (A, Figure 3) stays constant while that of the second (B, Figure 3) shifts with $h\nu$. A positive sample bias of ~1 V is used to reduce the secondary background in these spectra. We do not attempt to fit the features at energies lower than peak A. Within experimental uncertainty, this simplification does not affect the positions of peaks A and B in Figure 3. The same procedure is used to obtain peak positions in Figure 5 (see below). The lower panel in Figure 4 shows the positions of these two molecular resonances, which are obtained from the aforementioned decomposition procedure, as a function of photon energy. The data points can be fit by straight lines, with slopes of $n_A = 0.0 \pm 0.2$ and $n_B = 1.1 \pm 0.2$, respectively. Within experimental uncertainty, these two slopes are essentially 0 and 1, respectively. The two molecular resonances must correspond to electron transfer to a final state (above the vacuum level) and an intermediate state (between the Fermi and the vacuum level). These two states are located at 6.40 ± 0.05 and 3.30 ± 0.10 eV above the Fermi level, respectively.

To understand the nature of the two unoccupied states established above, we have compared results from the SAM of thiophenolates to those of alkylthiolates. Figure 5 shows a set of 2PPE spectra for an ethylthiolate SAM on Cu(111) taken at the indicated photon energies. They are very similar to those from the thiophenolate SAM. These spectra are again dominated by two peaks: one (A) remains constant with increasing photon energy, and the other (B) shifts with $h\nu$. Results from Gaussian decomposition are summarized in the top panel of Figure 4, where data points are peak positions and solid lines are least-squares linear fits. These fits yield slopes of $n_A = 0.0 \pm 0.2$ and $n_B = 1.0 \pm 0.2$. Thus, the two molecular resonances correspond to electron transfer to two unoccupied states: one above the vacuum level and the other between the Fermi and the vacuum level. They are located at 6.32 ± 0.05 and 3.31 ± 0.10 eV above the Fermi level, respectively. The work function of the C_2H_5S/Cu(111) surface is 3.70 eV.

Similar results are obtained for a SAM of octylthiolates on Cu(111), shown in Figure 6. Each spectrum can again be decomposed into two peaks (dashed curves, less resolved than those in Figure 5). As in Figure 2, a background function which provides an estimate to contribution from the tail of the secondary/d-band peak is used to facilitate the decomposition of each spectrum. Peak positions from Gaussian decomposition are shown, as a function of photon energy, in the middle panel in Figure 4. Least-squares linear fits to the data yield slopes of $n_A = 0.1 \pm 0.2$ and $n_B = 0.9 \pm 0.2$. The two unoccupied states are located at 6.37 ± 0.05 and 3.15 ± 0.10 eV above the Fermi level, respectively. The work function of the $C_8H_{17}S$/Cu(111) SAM covered surface is 3.50 eV. Note that at $h\nu = 2.88$ eV, these two unoccupied states are not accessible, as shown by the bottom spectrum in Figure 6.

3.2. The Common Origin Of Unoccupied States: The Cu−S−C Anchor. Table 1 summarizes the positions of the two unoccupied electronic states, along with the work function, in the three SAM systems. The positions of both states are nearly independent of the nature of the hydrocarbon group. We conclude that the observed molecular resonances in thiolate SAMs do not originate from the molecular framework, but rather from a common unit, i.e., the C−S−Cu linker.

Support of this assignment is found in the symmetry of the

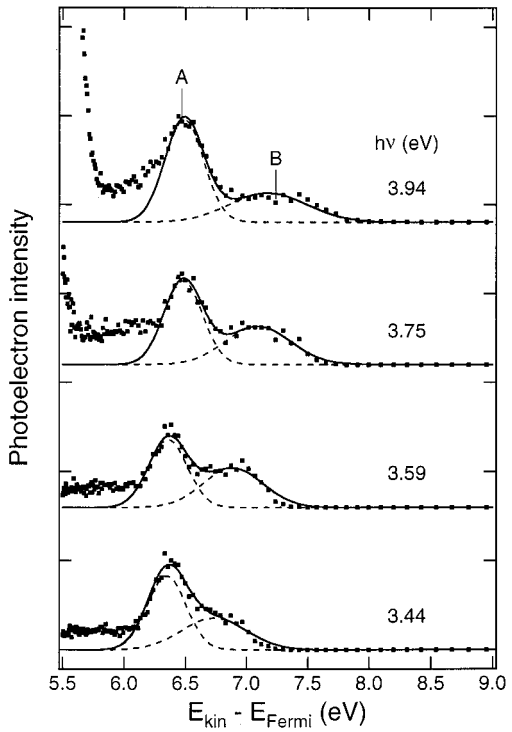

Figure 5. Two-photon photoemission spectra obtained for a self-assembled monolayer (SAM) of *n*-C_2H_5S/Cu(111) at the indicated photon energies (3.44−3.94 eV). Dots are experimental data points. The dashed curves (A and B) are from peak decomposition assuming Gaussian peak shapes and the solid curve is the sum of dashed curves. Note that background contribution on the lower energy side of each spectrum is not accounted for in the decomposition (see text for details).

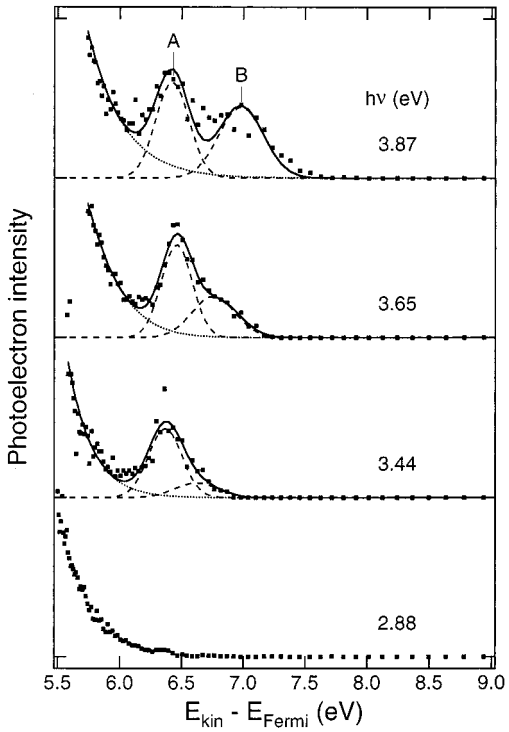

Figure 6. Two-photon photoemission spectra obtained for a self-assembled monolayer (SAM) of *n*-$C_8H_{17}S$/Cu(111) at the indicated photon energies (2.88−3.87 eV). Dots are experimental data points. The dashed curves (A and B) are from peak decomposition assuming Gaussian peak shapes and the solid curve is the sum of dashed curves. The dotted curves are estimated background functions used to facilitate fitting (see text for details).

Table 1. Work Functions and Positions of Unoccupied States (referenced to the Fermi level) for Each SAM

SAMs	work function	resonance A	resonance B
C_6H_5S/Cu(111)	3.70 ± 0.05 eV	6.40 ± 0.05 eV	3.30 ± 0.10 eV
n-C_2H_5S/Cu(111)	3.70 ± 0.05 eV	6.32 ± 0.05 eV	3.31 ± 0.10 eV
n-$C_8H_{17}S$/Cu(111)	3.50 ± 0.05 eV	6.37 ± 0.05 eV	3.15 ± 0.10 eV

optical excitation, which is determined from polarization dependence of the 2PPE signal. This approach has been used extensively in 2PPE literature to determine the symmetry of optical transitions on surfaces. There are two general scenarios in 2PPE. Photoemission can be induced by (1) sequential, direct optical transitions from an initial state, $|i\rangle$, to a final state, $|f\rangle$, and (2) an indirect mechanism in which an intermediate, unoccupied state, $|k\rangle$, is populated by the scattering of photo-excited substrate electrons, followed by a direct transition from $|k\rangle$ to $|f\rangle$. In both cases, the photoemission intensity is given by Fermi's golden rule and depends strongly on the orientation of the transition dipole moment and the electric field vector. For example, it is well-known that image states on metal surfaces are of σ symmetry and are excited by electric fields perpendicular to the surface.[20−22] Detailed formulation for the polarization dependence of 2PPE intensities involving adsorbates can be found in a recent publication by Wolf et al.[39] Figure 7 compares 2PPE spectra taken with p- (solid) and s- (dashed) polarized light for both the thiophenolate (upper) and the ethylthiolate (lower) SAMs. In each case, the two spectra have been normalized to give the same secondary electron intensity. In the C_6H_5S/Cu(111) system, the intensity ratio for p- and s-polarization is $I_p/I_s \approx 4$ for both resonances. For C_2H_5S/Cu(111), the ratio is $I_p/I_s \approx 3$. These results suggest that the optical transitions are of σ symmetry with transition dipole moments oriented close to surface normal. This is in agreement with σ^* states localized to the Cu−S−C anchor, as shown below.

We have also carried out dispersion measurement to establish the delocalization of electrons in these two unoccupied states. In this experiment, photoemitted electron is detected as a function of the angle between surface normal and the center axis of the TOF spectrometer. A plot of photoelectron peak position as a function of parallel momentum, $k_{||}$, reveals dispersion for both states, indicating that these electron transfer states are delocalized (data not shown). However, due to limitations of our sample and detector geometries, there were large uncertainties associated with these measurements. Thus, we were not able to reliably obtain effective electron masses in these delocalized states.

Note that the observed resonance, *B*, located at 0.35−0.40 eV below the vacuum level, is nearly independent of the structure of the hydrocarbon group. We believe this state cannot be attributed to an image state. The binding energy of the first image state ($n = 1$) on clean Cu(111) is 0.8 eV.[23] This binding energy changes in the presence of adsorbates. For example, the adsorption of benzene changes it from 0.9 eV at 1 ML to 0.65 eV at 2 ML.[29] Harris and co-workers carried out extensive investigations of image states on hydrocarbon covered metal surfaces and showed that the binding energy is sensitive to the nature of the hydrocarbon group and the thickness of the adsorbate layer.[21] As an example for the latter, the binding energy of the $n = 1$ image state on *n*-pentane-covered Ag(111) decreases from 0.7 eV at 1 ML to 0.45 eV at 3 ML adsorbate coverage. However, the binding energies (Table 1) of resonance B observed in self-assembled monolayers on Cu(111) are, within

(39) Wolf, M.; Hotzel, A.; Knoesel, K.; Velic, D. *Phys. Rev. B* **1999**, *59*, 5926.

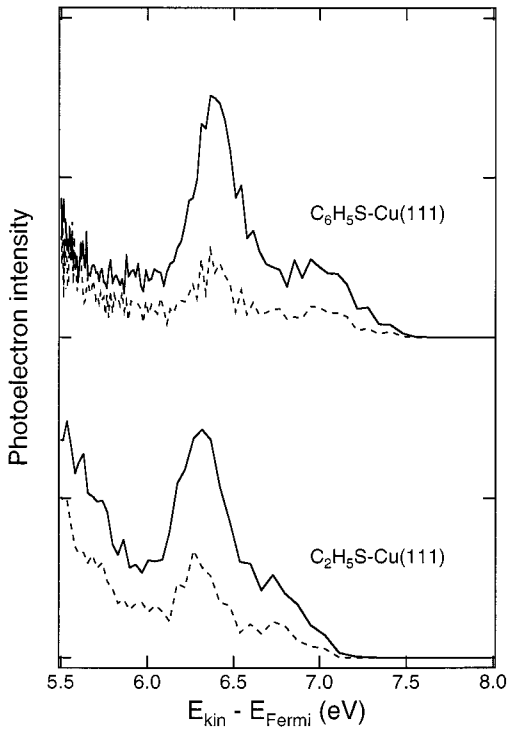

Figure 7. A comparison of two-photon photoemission spectra, under the irradiation of p (solid) and s (dashed) polarized light, for SAMs of *n*-C_2H_5S/Cu(111) (lower) and C_6H_5S/Cu(111) (upper). In each system, the two spectra are normalized to give the same secondary electron intensity. Photon energy: $h\nu = 3.44$ and 3.70 eV for *n*-C_2H_5S/Cu(111) and C_6H_5S/Cu(111), respectively. Results are similar at other photon energies.

experimental uncertainty, independent of the nature of the hydrocarbon group (phenyl vs alkyl) or the thickness of the layer (ethyl vs octyl). We believe this spectral feature is dominated by a molecular resonance.

3.3. Molecular Orbitals and the Nature of the Interfacial Electronic Structure. To better understand the nature of the two unoccupied states established above by the 2PPE experiments, we first carried out ab initio calculations on two very simple model systems: copper(I) thiophenolate and copper(I) propanethiolate. Neutral molecular geometries were fully optimized at the B3LYP level of electronic structure theory,[40,41] using the cc-pVDZ basis set for H, C, and S,[42,43] and the all-electron polarized double-ζ basis set of Schafer et al.[44] for Cu (this combination will be referred to as pVDZ). The neutral structures, both of which belong to the C_s point group, were established as local minima by calculation of analytical force constants.

Table 2 summarizes the predicted energetics associated with removing an electron from the highest occupied molecular orbital (HOMO) and attaching an electron to either the LUMO or the LUMO+1 orbitals for the two model systems. In spectroscopic notation, these processes are represented as $1^2A''^+ \leftarrow 1^1A'$, $1^2A'^- \leftarrow 1^1A'$, and $2^2A'^- \leftarrow 1^1A'$, respectively, where the energy changes associated with the first and second processes are commonly referred to as the ionization potential (IP) and the electron affinity (EA) — we emphasize that we are here considering *vertical* processes. For these single-point calculations the basis sets employed were aug-cc-pVDZ for H, C, and S,[42,43] and for Cu the basis set of Schafer and co-workers was augmented with one set each of diffuse s, p, and d functions having exponents of 0.009, 0.042, and 0.100, respectively (this combination will be referred to as pVDZ+).[44]

Table 2. Energies (eV) for Vertical Ionization of and Electron Attachment to Copper Thiolates[a]

R−S−Cu	$1^2A''^+ \leftarrow 1^1A'$(IP)[b]	$1^2A'^- \leftarrow 1^1A'$(EA)[b]	$2^2A'^- \leftarrow 1^1A'$[c]
R = C_6H_5[d]	7.3	1.3	−1.1
R = *n*-C_3H_7[e]	7.9	1.0	−1.3

[a] Positive ionization energies correspond to endoergic processes. Positive electron attachment energies correspond to exoergic processes. All energies from B3LYP/pVDZ+ calculations for B3LYP/pVDZ neutral geometries. [b] Calculated as ΔE_{SCF}. [c] Calculated as EA − $(\epsilon_{LUMO+1} - \epsilon_{LUMO})_{neutral}$. [d] Neutral electronic energy: −2270.245 61 hartrees. [e] Neutral electronic energy: −2157.120 43 hartrees.

Since the $1^2A''^+ \leftarrow 1^1A'$ and $1^2A'^- \leftarrow 1^1A'$processes involve only ground states of a given charge and state symmetry, the energy differences are readily calculated as differences in B3LYP self-consistent-field (SCF) energies from Kohn−Sham wave functions optimized for the respective states (ΔE_{SCF}). The SCF energy of the $2^2A'^-$ state, on the other hand, is not so simply determined; the LUMO+1 belongs to the same irreducible representation as the LUMO (a′), and trial SCF wave functions for this excited state inevitably collapsed to the wave function for the ground $1^2A'^-$ state; such behavior is expected for any single determinantal method.[45] Thus, Table 2 computes the energy for the $2^2A'^- \leftarrow 1^1A'$ process as the EA minus the difference in energy between the LUMO and the LUMO+1 orbitals of the neutral.

To provide some estimate of the accuracy of this approach, we calculated the energy change for the $1^2A''^- \leftarrow 1^1A'$ process in a different model system, lithium thiophenolate. The $1^2A''^-$ state derives from population of the lowest energy π^* orbital of the aromatic ring, which is the LUMO+2 of this system and belongs to the a″ irreducible representation. Since this state is not the ground state of the radical anion, but is the lowest energy state of A″ symmetry, we can calculate the electron attachment energy using both the ΔE_{SCF} and EA minus orbital energy difference methods. In this particular model system, using equivalent levels of theory, the two methods agree within 0.3 eV, which may be taken as a reasonable estimate of the error associated with use of the latter method in Table 2.

The data in Table 2 indicate that the ionization and electron attachment energies are relatively insensitive to the nature of the R group attached to sulfur in the thiolate linker. This may be understood from inspection of the relevant HOMO, LUMO, and LUMO+1 orbitals in the model systems (Figure 8). The HOMOs for both models belong to the a″ irreducible representation. For copper(I) propanethiolate, the HOMO is dominated by contributions from a sulfur 3p orbital, with some delocalization over a copper 3d orbital, and a combination of C−H σ orbitals on the carbon attached to sulfur. In copper(I) thiophenolate, the HOMO is more delocalized, involving again a sulfur 3p orbital, but now mixing with the highest occupied π orbital associated with the aromatic ring.

The LUMO and LUMO+1 orbitals, on the other hand, are both well described as σ^*-type orbitals. The LUMO in both model systems corresponds cleanly to a σ^*_{CuS} orbital. The LUMO+1 in both model systems derives from a roughly equal

(40) Becke, A. D. *J. Chem. Phys.* **1993**, *98*, 5648.
(41) Stephens, P. J.; Devlin, F. J.; Chabalowski, C. F.; Frisch, M. J. *J. Phys. Chem.* **1994**, *98*, 11623..
(42) Dunning, T. H. *J. Chem. Phys.* **1989**, *90*, 1007.
(43) Woon, D. E.; Dunning, T. H. *J. Chem. Phys.* **1993**, *98*, 1358.
(44) Schafer, A.; Horn, H.; Ahlrichs, R. *J. Chem. Phys.* **1992**, *97*, 2571.

(45) Even if one could induce convergence to a $^2A'^-$ wave function of higher energy than the ground state, the Kohn−Sham theorem provides no formal guarantee that a functional of the density exists from which the correct electronic energy may be calculated. See ref 46.

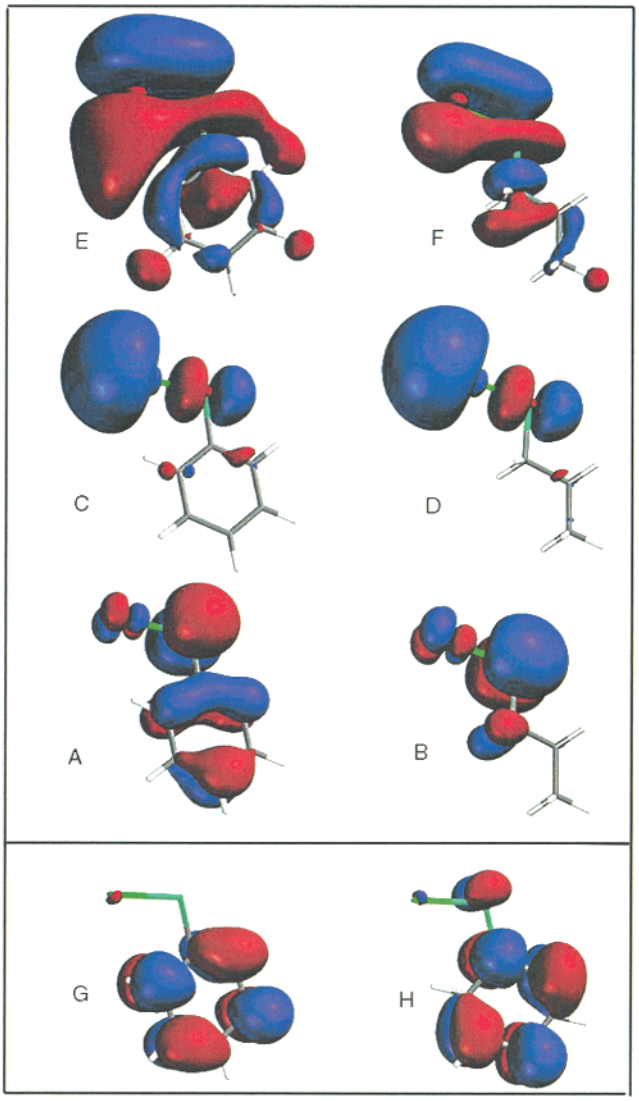

Figure 8. Upper panel: (A, C, E) HOMO, LUMO, and LUMO+1 molecular orbitals for copper(I) thiophenolate; (B, D, F) HOMO, LUMO, and LUMO+1 molecular orbitals for copper(I) propanethiolate. Lower panel: (G and H) two π^* molecular orbitals for copper(I) thiophenolate. The orbital energies (E_h) at the B3LYP/pVDZ+ level are: (A) −0.20313; (B) −0.20852; (C) −0.11298; (D) −0.10374; (E) −0.02472; (F) −0.01896;(G) −0.02384; and (H) −0.01234.

combination of a σ^*_{CS} orbital and a π_{CuS} orbital with some incidental contributions from orbitals localized on other atoms. In each virtual orbital, then, there is a substantial contribution from copper atomic orbitals.

To improve on the quality of the computational model systems, we performed further B3LYP/pVDZ calculations including an additional two copper atoms (Figure 9). The three copper atoms were constrained to occupy the vertexes of an equilateral triangle having a side length equal to the copper−copper spacing in bulk copper metal (2.56 Å). The thiolates were allowed to bond either to an edge of the triangle, with the remaining copper atom "below the surface", or to the face of the triangle (isomer **c**), subject to the constraint that the two Cu−S distances in the edge case, and the three Cu−S distances in the face case, were individually equal to one another; all other degrees of freedom were optimized. In the edge case, parallel (isomer **a**) and perpendicular (isomer **b**) orientations of the plane containing the heavy atoms of the organic fragment relative to the copper triangle were considered — the two orientations differ from one another by less than 0.01 eV with the perpendicular

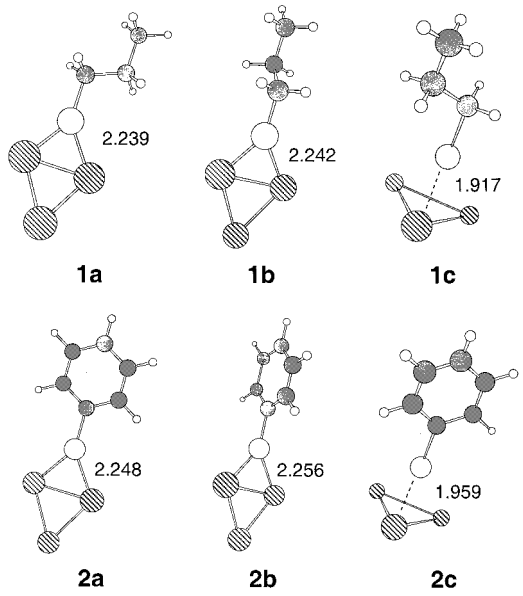

Figure 9. B3LYP/pVDZ structures for thiolates complexed to 3 copper atoms. Cu−S bond lengths are indicated for isomers **a** and **b** and the normal distance between S and the plane of the copper atoms is indicated for isomers **c** (angstroms). Absolute energies (hartrees): **1a**, −5437.78876; **1b**, −5437.78912; **1c**, −5437.76533; **2a**, −5550.91238; **2b**, −5550.91205; and **2c**, −5550.88757. All calculations were carried out using the Gaussian 98 program package.[50]

being the lower in energy for the propyl case (structure **1**) and the parallel being lower for the phenyl case (structure **2**). For practical purposes, then, there may be considered to be free rotation about this degree of freedom. Thus, we will focus interpretation on both edge-coordinated isomers simultaneously.

The relative energies for the edge vs face coordination motifs, on the other hand, are very different. In each case, coordination to the face is more than 0.6 eV higher in energy than coordination to the edge, suggesting that SAMs will strongly prefer the former arrangement. Given the higher energy of the **c** isomers and the precedent established for the **a** and **b** isomers, we did not examine rotation of the organic fragment about the surface normal vector in isomers **c**.

An analysis of the virtual orbitals in the tricopper models offers a similar picture to that for the monocopper models, with some slight complications. One complication is that extra copper atoms necessarily bring in virtual orbitals that form the beginning of the empty part of the copper conduction band, and these intervene between the orbitals analogous to LUMO and LUMO+1 in Figure 8.

In the edge-coordinated structures, the cluster LUMOs do retain their character as virtual orbitals that are net Cu−S antibonding for both the propyl and phenyl cases. Because of the nature of sulfur's interaction with two copper atoms instead of one, the orbitals in question are 3-center orbitals (and thus not as appropriately described as σ^* orbitals) but they are otherwise analogous to the LUMOs of the monocopper systems in Figure 8. At higher energy, above two virtual orbitals that are localized almost entirely on the "uncoordinated" copper atom of the triangle, σ^*_{CS} orbitals closely resembling those in Figure 8 are again found in each case. The energy separation between the relevant pairs of virtual orbitals is predicted to be 2.8 and 2.9 eV for **1a** and **1b**, respectively, and 3.1 and 3.0 eV for **2a** and **2b**, respectively. These energy separations improve upon the results obtained in the monocopper model systems (Table 2), and are now in very close agreement with the gap of 3.1 eV observed experimentally.

In the phenyl case, the two low-energy π^* orbitals associated with the aromatic ring now lie very slightly below the σ^*_{CS} orbital, instead of very slightly above, as in the monocopper system, but these π^* orbitals continue to have essentially negligible localization on copper atoms. This low overlap between π^* and copper orbitals is consistent with the failure of experiment to detect corresponding virtual states.

The face-coordinated tricopper systems are probably not relevant to the experimental situation, given their high energy relative to edge-coordinated isomers, but we present an analysis of their virtual orbitals for completeness. The local 3-fold symmetry of the Cu−S interactions causes the two lowest energy orbitals of the cluster to be essentially a degenerate pair, each well characterized as being net antibonding between copper and sulfur. For this case, then, the geometry of the system does not permit any separation of nascent band structure from specific copper−sulfur orbitals. Above this degenerate pair, the σ^*_{CS} orbitals are again found for each case, and they closely resemble those depicted in Figure 8. However, in the face-coordinated systems the energy separation between the relevant pairs of virtual orbitals is only 1.6 and 1.7 eV for the propyl and phenyl cases, respectively.

With all of these theoretical results as a guide, we assign the two virtual states observed in the 2PPE spectra as deriving from population of the corresponding virtual orbitals described above. This assignment is based on the following observations: (1) the energies of the virtual states accessed in the 2PPE experiment are insensitive to a particular choice of R group, and theory indicates the low-energy σ^*-like orbitals to have little delocalization onto R-group atoms (Figure 8). (2) The energetic spacing between the two virtual states is measured to be 3.1 ± 0.1 eV − theory estimates 2.8−3.1 eV. (3) Theory predicts the LUMO and LUMO+1 states in the model systems to be below and above the vacuum level, respectively, in agreement with 2PPE results. (4) Polarization measurements (Figure 7) suggest that both virtual states are of σ character, consistent with the shapes of the relevant virtual orbitals in the model systems.

Concluding this section, we note that for copper(I) thiophenolate, there *are* two unoccupied orbitals close in energy to the σ^*_{CS} orbital both of which belong to the a″ irreducible representation and are well described as aromatic ring π^* orbitals having negligible delocalization onto copper (lower panel, Figure 8). Excitation into these orbitals is not observed, however, probably because of the low overlap with metal bands. The limited energy resolution in experiments is another factor.

3.4. Implication for SAMs of Molecular Electronics. Self-assembly of thiolates on metal surfaces has attracted considerable attention in recent studies on molecular electronics. Consider a simple case of a conjugated molecule connected between two metal electrodes via thiolate (−S−metal) linkages. Two major factors control current flow in this circuit: the internal molecular structure and molecule−metal contacts, i.e., thiolate linkages. The first factor has been extensively investigated both experimentally and theoretically.[47−49] We focus on the second factor here. Our two-photon photoemission measurements and computational results indicate that unoccupied states at the interfaces are dominated by two virtual states associated with the SAM. The lower energy state is net antibonding between S and the surface while the higher energy state is well described as a σ^*_{CS} orbital. These two states are localized to the −C−S−Cu anchoring group and strongly coupled to the metal substrate. Calculations also predict that π^* states in conjugated molecules are largely isolated from the metal surface (see the lower panel in Figure 8) while the π HOMO is delocalized over the molecule and the metal surface via the S linker.

In electron conduction through a conjugated molecule connected at both ends via thiolates to metal electrodes, molecular states close to metal Fermi levels make dominant contributions to conductance. Both HOMO and LUMO within the molecule are important, depending on their relative positions to Fermi levels and the bias voltage.[14,17] However, the role of contact resistance can be different for the two molecular states. When the delocalized π HOMO dominates the conduction mechanism, as in hole transport, contact resistance is likely insignificant because the π HOMO is strongly coupled to metal surfaces via sulfur bridges. In contrast, when the virtual states are more important, as for electron transport, conductance is likely limited by insulation between thiolate contacts. Although π^* states are well delocalized over the entire molecule in conjugated "molecular wires", there is little delocalization of the molecular π^* states over the −S− linkage and the metal substrate. The interface is dominated by two virtual states localized to the thiolate group. Computational results on model molecules indicate that the delocalized π^* within the conjugated molecular framework may not couple strongly to the localized virtual states at the interface. Thus, these localized virtual states may not serve as efficient "bridge states", using the language of intramolecular long-range electron transfer.[47−49] We may view the interface as an insulating barrier and electron conduction may involve tunneling between the molecular π^* and metal band structures.

4. Conclusions

Two-photon photoemission has been used to probe interfacial electronic structures, particularly unoccupied states, in self-assembled monolayers of thiolates on Cu(111). The interpretation of experimental results is assisted by ab initio calculations of model molecules/clusters. We found that the interfacial electronic structure is dominated by two virtual states localized to the C−S−Cu anchor and strongly coupled to the metal substrate. These interfacial states, located at ∼0.4 eV below and 2.7 eV above the vacuum level, respectively, are independent of the nature of the hydrocarbon group (conjugated aromatics or saturated alkyls). The implication of this finding for self-assembled molecular electronics is that, while thiolate contacts may be conducting for conjugated molecular wires when hole transport is important, they can be insulating when electron transport dominates.

Acknowledgment. X.Y.Z. acknowledges support by the University of Minnesota, Research Corporation, the Petroleum Research Fund administrated by the American Chemical Society, and the National Science Foundation. C.J.C. acknowledges support by the Alfred P. Sloan Foundation.

Supporting Information Available: Listing of absolute energies and geometries and for all stationary points vibrational frequencies and orbital energies (PDF). This material is available free of charge via the Internet at http://pubs.acs.org.

JA993486W

(46) Gunnarsson, O.; Lundqvist, B. I. *Phys. Rev. B* **1976**, *13*, 4274.
(47) Closs, G. L.; Miller, J. R. *Science* **1988**, *240*, 440.
(48) Mujica, V.; Kemo, M.; Ratner, M. A. *J. Chem. Phys.* **1994**, *101*, 6849.
(49) Bixon, M.; Jortner, J. *J. Chem. Phys.* **1997**, *107*, 5154.
(50) Frisch, M. J.; Trucks, G. W.; Schlegel, H. B.; Gill, P. M. W.; Johnson, B. G.; Robb, M. A.; Cheeseman, J. R.; Keith, T. A.; Petersson, G. A.; Montgomery, J. A.; Raghavachari, K.; Al-Laham, M. A.; Zakrzewski, V. G.; Ortiz, J. V.; Foresman, J. B.; Peng, C. Y.; Ayala, P. A.; Wong, M. W.; Andres, J. L.; Replogle, E. S.; Gomperts, R.; Martin, R. L.; Fox, D. J.; Binkley, J. S.; Defrees, D. J.; Baker, J.; Stewart, J. P.; Head-Gordon, M.; Gonzalez, C.; Pople, J. A. *Gaussian 98;* Gaussian, Inc.: 1998.